ELSEVIER

Process Biochemistry 42 (2007) 812–819

Process Biochemistry

www.elsevier.com/locate/procbio

Dual fluorescence confocal imaging of the accessibility and binding of $F(ab')_2$ to an EBA resin with various immobilised antigen densities

Rihab Boushaba *, Clemens F Kaminski, Nigel KH Slater

Department of Chemical Engineering, University of Cambridge, Pembroke Street, Cambridge CB2 3RA, UK

Received 6 July 2006; received in revised form 8 January 2007; accepted 29 January 2007

Abstract

Dual fluorescence confocal laser scanning microscopy has been used to visualise the binding of a fluorescently labelled polyclonal ovine anti-fluorescein $F(ab')_2$ antibody to immobilised fluorescein. The fluorescent ligand was immobilised on a Streamline quartz base agarose matrix; a resin used industrially for expanded bed chromatography, using two different fluorescein initial concentrations in order to obtain two batches of immunogen-affinity adsorbent with different immobilised ligand densities. The fluorescein specific $F(ab')_2$ were purified from anti-fluorescein serum pepsin digest by adsorption on immobilised antigen chromatographic resin, followed by conjugation to the fluorescent probe Alexa Fluor 660. The dual fluorescence signals from the immobilised antigen and the immuno-specific $F(ab')_2$ were used to map the progressive depth of the bound $F(ab')_2$ layer within individual adsorbent beads. In addition, the labelled anti-fluorescein $F(ab')_2$ was diluted to identical antigen binding activity concentrations in crude serum digest and in blank buffer and the resulting fluorescence intensity profiles were comparatively assessed for any detectable differences in binding patterns that might be caused by processing the more complex mixture of crude serum digests. It was observed that the relative immobilised ligand utilisation was higher when using the immuno-adsorbent with lower immobilised antigen density. Furthermore, the progression of the adsorbed $F(ab')_2$ front inside the immuno-adsorbent beads displayed closer agreement with the postulates of the shrinking core mechanism (SCM) when the immuno-adsorbent with lower immobilised antigen was used. The confocal images did not reveal any differences between the depth of the adsorption fronts of crude serum digest and pre-purified $F(ab')_2$ samples.

Keywords: Confocal scanning laser microscopy; $F(ab')_2$; Fluorescein; Immuno-affinity chromatography; Adsorbent; CSLM

1. Introduction

The specificity shown by polyclonal IgG's and their active Fab or $F(ab')_2$ fragments towards their corresponding antigens makes them ideal for many therapeutic applications [1]. Purification of $F(ab')_2$ fragments may be achieved by precipitation (ammonium sulphate or caprylic acid [2]) or chromatographic methods [3–5]. Several ways have been proposed to improve the purity and neutralising efficiency of $F(ab')_2$ fragments and to increase their safety [5,7]. However, many of these have resulted in minor improvements in $F(ab')_2$ quality and higher cost of production due to their reliance upon chromatography [8].

Antigen immuno-affinity chromatography is one way of ensuring an antibody product of high specific activity, as it is highly selective towards the sub-population of antibodies directed towards the antigen of interest. The possible advantages of the use of affinity ligands in expanded bed adsorption (EBA) have been reported by a number of authors; in particular, the combination of EBA as a direct recovery operation with the enhanced selectivity of affinity ligands may prove in some cases to be the most efficient method for the selective capture of the target product from complex feedstocks [9]. Streamline matrices were developed by Amersham Biotech with the purpose of allowing the formation of stable fluidised beds at high operating flow velocities. Streamline beads are inter-dispersed with inert quartz particles in order to increase the settling velocity of the matrix and increase its mechanical rigidity. These quartz particles introduce a higher degree of non-homogeneity compared with regular chromatographic adsorbents such as Sepharose.

In the present study, a dual fluorescence antibody-antigen system was used in order to visualise the accessibility of Alexa Fluor 660-labelled anti-fluorescein antibody fragments $F(ab')_2$ to

* Corresponding author.
E-mail address: r.boushaba@ucl.ac.uk (R. Boushaba).

1359-5113/$ – see front matter
doi:10.1016/j.procbio.2007.01.017

immobilised fluorescein inside epoxy-activated agarose Streamline beads by means of confocal microscopy. The fluorescence intensity profiles of immuno-affinity adsorbents carrying two different immobilised ligand loadings were compared in order to develop insights on the spatial distribution of the bound anti-fluorescein $F(ab')_2$ fragments in the two cases. Confocal scanning laser microscopy has been demonstrated by several published studies to be a useful technique for visualising binding events inside chromatographic matrices due to its high resolution characteristic [10]. However, the majority of the studies achieved on chromatographic matrices have centred on homogeneous gel phase adsorbents such as Sepharose [10]; which are more useful for packed bed chromatography operations. Less homogeneous adsorbent such as Streamline matrices are more challenging to characterise using confocal microscopy, however the high resolution power of confocal microscopy might still be used to compare the binding of a target protein to various batches of Streamline adsorbent containing different immobilised ligand loadings. To achieve this, we have used the fluorescein/anti-fluorescein $F(ab')_2$ system since it allows the visualisation of the binding process via two independent fluorescence processes: (i) fluorescence quenching of fluorescein resulting from binding of anti-fluorescein $F(ab')_2$ to the immuno-affinity adsorbent and (ii) fluorescence of the bound Alexa Fluor 660-conjugated anti-fluorescein $F(ab')_2$. This dual fluorescence detection method allowed the visualisation of immobilised ligand usage relative to the immobilised ligand density on the beads by imaging two types of immuno-affinity adsorbents having different immobilised fluorescein concentrations.

This work followed on from previous studies which were concerned with the assessment of disposable process technology as a less expensive alternative to traditional packed bed chromatography, for the manufacture of therapeutic $F(ab')_2$ fragments [11]. Magnetisable beads were used to synthesise the chromatographic adsorbent, which was subsequently introduced aseptically into disposable bio-processing bags containing the $F(ab')_2$-rich serum digest (resulting from a pepsin proteolysis step). The purification of $F(ab')_2$ was thus performed in batch-mode, with the separation of the solid phase being achieved by the application of a magnetic field in order to rapidly sediment the adsorbent beads. Streamline adsorbent was used in these studies because its design makes it inherently suited for applications where good fluidisation properties, mechanical rigidity and rapid settling velocities are essential; such as in the case of bioprocessing in disposable bags.The study described herein aimed at using confocal imaging in order to gain further insights on the binding characteristics of the $F(ab')_2$ under these batch purification conditions and therefore finite batch experiments were carried out as opposed to the more traditional packed bed configuration.

2. Materials and methods

2.1. Materials

Streamline agarose quartz matrix, PD-10 Sephadex G-25 columns and high resolution Superose 12 10/30 HR column for size exclusion chromatography were purchased from GE Healthcare (formerly Amersham Biosciences) (Amersham, UK). FLEXBOY® pre-sterilised, disposable bio-processing bags were a generous gift from Stedim (Aubagne, France). Ultra-filtration membranes Vivaflow 50 were purchased from Sartorius Ltd. (Epsom, UK). Alexa Fluor 660 succinimidyl ester and Fluorescein-5-thiosemicarbazide were purchased from Invitrogen (formerly Molecular Probes) (Leiden, Netherlands). Sheep anti-fluorescein serum and anti-fluorescein-free serum were supplied by Micropharm Ltd. (Emlyn, UK). Pepsin and all other reagents were obtained from Sigma–Aldrich Company Ltd. (Gillingham, UK).

2.2. Instrumentation

Confocal microscopy analysis was performed with an Olympus/FluoView FV300 laser scanning microscope (Olympus, UK) equipped with a multi-line Argon ion laser and red and green Helium neon lasers as excitation sources. Up to 3 detection channels could be acquired simultaneously. Image acquisition and analysis were performed using the built-in Olympus Fluoview software. Each image was the result of an overlay of the images obtained in the two fluorescence channels corresponding to fluorescein (ligand) emission and Alexa Fluor 660 emission ($F(ab')_2$).The detection settings were kept constant for both batches of adsorbents to allow direct comparison to be made between the depth of penetration of the labelled anti-fluorescein $F(ab')_2$ in the case of high immobilised ligand load and low immobilised ligand load. Therefore, only the fluorescence emitted by the Alxa Fluor 660 dye was used to estimate the penetration depths. The fluorescence of the immobilised ligand was only used to visualise the immobilised ligand distribution within the adsorbent particles.

2.3. Preparation of immuno-affinity adsorbent

Agarose Streamline quartz base matrix was epoxide activated by reaction with oxirane 1,4-butanediol diglycidyl ether in 2:1 (v/v); according to the method described by Sundberg and Porath [12]. Activated agarose beads were washed with distilled water and subsequently reacted with solutions of an amine-derivative analogue of fluorescein (fluorescein-5-thiosemicarbazide). Fluorescein-5-thiosemicarbazide was used in solutions of 6.25 or 0.625 mM concentrations, prepared in 0.5 M sodium carbonate pH 11.0. Throughout the manuscript, fluorescein-5-thiosemicarbazide will be referred to as fluorescein for simplicity. The mixtures were incubated at 37 °C for 18 h. Blocking of unreacted active sites was achieved by adding 2 volumes of 1 M ethanolamine pH 10.0 and incubating overnight at 25 °C. The adsorbent was washed with 0.5 M sodium carbonate + 0.15 M NaCl, then with 50 mM glycine-HCl, pH 2.5 and finally with 10 mM sodium phosphate + 0.1 M NaCl, pH 8.0. The extent of fluorescein immobilisation was determined from the absorbance of the supernatant solutions at 491 nm. Two sets of immuno-affinity adsorbents were synthesised in this way, a high ligand loading adsorbent with 8.2 μmol immobilised fluorescein/mL beads and a low ligand loading adsorbent with 0.92 μmol immobilised fluorescein/mL beads.

2.4. Preparation of anti-fluorescein $F(ab')_2$ by pepsin digestion and immuno-affinity

Whole hyperimmune serum from sheep was diluted in 2 volumes of 20 mM glycine-HCl and the pH adjusted to pH 3.5 with 1 M HCl. Pepsin lyophilised powder was added at a ratio of 1:25 mg pepsin/mg protein, where the protein content of serum was determined with the Bradford assay. The mixture was incubated at 37 °C for 16 h, after which the proteolysis reaction was terminated by the addition of 1 M Tris and raising the pH to 7.0; at which pH pepsin is irreversibly inactivated. The digestion efficiency was visualised using SDS-PAGE of digested serum as compared with whole undigested serum and the results were published elsewhere [13]. The digest was filtered and diluted with 2 volumes of 10 mM sodium phosphate + 0.1 M NaCl, pH 7.0. A volume of 2 L of this serum digest solution was pumped into a 5 L capacity FLEXBOY® pre-sterilised bag and 45 mL immuno-adsorbent with 0.92 μmoles immobilised fluorescein/mL beads were injected. The batch mixture was incubated for 2 h with gentle mixing, after which the supernatant solution was filtered and the immuno-adsorbent beads were washed with sodium phosphate buffer until no detectable absorbance at 280 was noted on spectrophotometer readings of the wash supernatant. Elution of bound $F(ab')_2$ was carried out by the addition of

1 L of 75 mM glycine-HCl, pH 2.0 and incubation for 10 min at room temperature with gentle mixing. The eluate solution pH was immediately raised to pH 4.0 by the addition of 1 M NaOH (higher pH resulted in aggregation). The recovered eluted protein solution was then extensively filtered and concentrated 50-fold using a Vivaflow 50 ultra-filtration membrane. The final sample concentration was 20 mg/mL as measured by the Bradford assay.

2.5. Fluorescent labelling of anti-fluorescein F(ab′)$_2$

A 10 mg/mL solution of immuno-affinity purified anti-fluorescein F(ab′)$_2$ was prepared by diluting the initial 20 mg/mL solution in 1 volume of 0.1 M sodium bicarbonate to raise the pH to within the range 7.5–8.5. Alexa Fluor 660 reactive red (5 mg) was dissolved in 0.5 mL *N*,*N*-dimethyl formamide and vortexed to obtain a 10 mg/mL reactive dye solution. While stirring the protein solution (10 mL total volume), 0.5 mL of the reactive dye solution was added slowly. The reaction mixture was incubated for 1 h at room temperature with continuous stirring. The conjugate was then immediately passed through a PD-10 Sephadex G-25 size exclusion chromatography column to separate labelled protein from excess un-conjugated dye. The degree of labelling (DOL) was measured according to the manufacturer's instruction and was found to be 2.6.

2.6. Confocal microscopy experiments

Confocal laser scanning microscopy was used to image the binding of anti-fluorescein F(ab′)$_2$ to two different ligand densities (immobilised fluorescein). Typically 60 image slices (512 pixels × 512 pixels) were obtained for each beads sample, spaced at 0.5 μm. Only the central slice near the maximum diameter of each bead image was used for further image analysis and all images presented in this paper represent these central slices. The resolution of the measurements was approximately 0.5 μm laterally and 1 μm in the z direction.

Two factors were investigated: (i) the immobilised fluorescein ligand density on the beads and (ii) the presence of the complex mixture of serum digest fragments that resulted from the pepsin digestion of whole serum to generate F(ab′)$_2$. To visualise the effect of immobilised ligand density on the depth of the bound F(ab′)$_2$ layer, 1 mL of immuno-affinity purified F(ab′)$_2$ samples (described in Section 2.4) were added to 100 μL of immobilised fluorescein agarose beads of different immobilised fluorescein densities (8.2 μmol immobilised fluorescein/mL beads and 0.92 μmol immobilised fluorescein/mL beads). In the case of investigating the effect of the presence of the complex serum digest components, the immuno-affinity purified anti-fluorescein F(ab′)$_2$ was conjugated to Alexa Fluor 660 reactive red as described in Section 2.5 and dissolved in two different buffers to the same final concentration of 20 μM anti-fluorescein F(ab′)$_2$. The first buffer was pure filtered sodium phosphate buffer (10 mM + 0.1 M NaCl, pH 8.0) and the second buffer was anti-fluorescein-F(ab′)$_2$-free serum digest in 10 mM sodium phosphate + 0.1 M NaCl, pH 8.0. Samples of 1 mL were subsequently contacted with 100 μL of adsorbent (0.92 μmol immobilised fluorescein/mL beads) for different time intervals. Only the adsorbent with 0.92 μmol immobilised fluorescein/mL beads was used in these experiments. All mixtures were incubated at room temperature, in the dark, with gentle mixing and 5 μL samples containing beads were withdrawn at pre-determined time intervals in each case. The particles were re-suspended in excess blank sodium phosphate buffer and extensively washed to discard any unbound protein solution. The washed, re-suspended beads were imaged using confocal microscopy.

The fluorescence emission was detected in 2 channels separately. The first channel detected the immobilised fluorescein fluorescence from within the adsorbent beads (green fluorescence; excitation at 457 nm; detection 515–550 nm) and the second channel detected the fluorescence of the Alexa Fluor 660 that was conjugated to the anti-fluorescein F(ab′)$_2$ (red fluorescence; excitation at 633 nm; detection at >660 nm). The large separation between absorption and emission spectra of the two fluorescent marker dyes resulted in minimal spectral overlap in the detected image channels and thus allowed a clear differentiation between the free fluorescein ligand sites and the bound Alexa Fluor 660-labelled antibody fragments on the beads. The images were therefore an overlay of the scans obtained in the two separate channels.

2.7. Image analysis of confocal microscopy data

The fluorescence intensity profile of the fluorescein ligand and the Alexa Fluor 660-labelled anti-fluorescein F(ab′)$_2$ across horizontal cross-sections of the beads were compiled for each time interval using Fluoview Image Analysis software. Up to 4 scans of (typically) 3 different beads were acquired. The depth of penetration of the fluorescently-labelled anti-fluorescein F(ab′)$_2$ was monitored in beads of comparable sizes, in order to minimise any heterogeneity effects resulting from disparity in bead sizes. To check for any background fluorescence resulting from binding of protein to the un-derivatised adsorbent; control experiments were carried out by incubating Streamline agarose and epoxy-activated Streamline agarose with Alexa Fluor 660-labelled F(ab′)$_2$ and imaging sample beads after washing. Insignificant fluorescence was detected in either case (data not shown).

3. Results and discussion

Fig. 1 shows images of a single Streamline agarose bead detected in 3 channels. In Fig. 1(a), an image of a single bead containing the immobilised fluorescein ligand (8.2 μmol immobilised fluorescein/mL beads) is shown, emitting at approximately 520 nm. It can be seen on the image that fluorescein is immobilised on the outer surface of the quartz

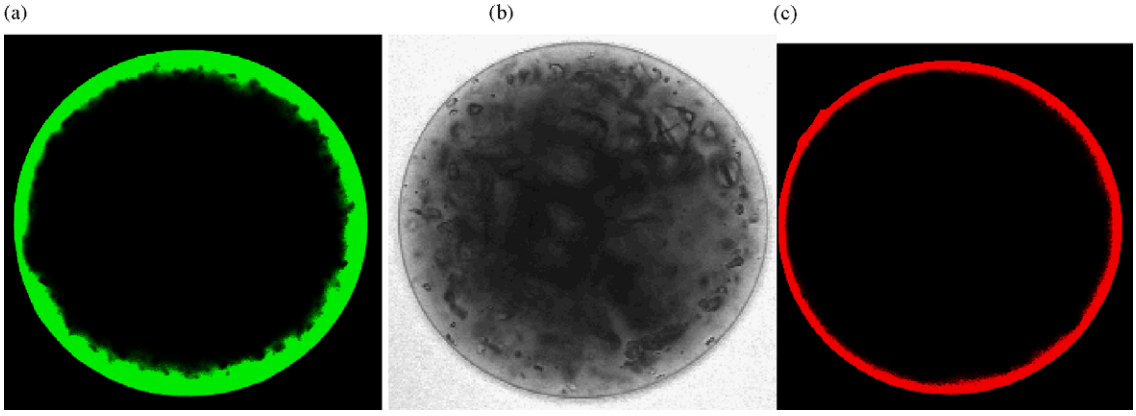

Fig. 1. Confocal microscope imaging of a plane near the centre of a single Streamline agarose bead with immobilised fluorescein after 60 minutes binding of Alexa Fluor 660, anti-fluorescein F(ab′)$_2$. (a) Fluorescein channel (green) exhibiting confinement of fluorescein near the surface of the bead. The inert central core of the bead appears dark as no immobilisation of the ligand takes place in this region. (b) Direct light optical image of the same bead. (c) Alexa 660 channel (red): The bound protein layer encircling the immuno-affinity adsorbent bead is clearly revealed by the technique.

adsorbent with the dark inner region corresponding to the inert central core. Fig. 1(b) shows a direct optical light transmission image of the same bead whilst Fig. 1(c) shows the binding of Alexa Fluor 660-labelled anti-fluorescein $F(ab')_2$ to the immobilised fluorescein on the bead surface via the detection of the fluorescence of the Alexa Fluor 660 dye. It can be seen from these images that fluorescein is immobilised on the outer surface of the quartz-based Streamline adsorbent, which contains an inert central core appearing in black due to the absence of fluorescence resulting from immobilised fluorescein. The black core in the images shown in Fig. 1(a) and (b) are not an indication of uneven immobilisation of the fluorescein ligand. The chromatographic matrix that was used in this work contains a quartz-based inert core in order to facilitate its fluidisation and sedimentation in batch-mode and expanded bed applications, for the purposes of which it was designed [14]. By incorporating this dense inert core, the protein diffusion resistance inside the adsorbent is effectively reduced due to shortening of the diffusion path and the resulting heavier beads have more stable fluidisation properties. However, this inert core remains inaccessible for protein adsorption or ligand immobilisation applications and hence it showed as a black, fluorescence-free region in the images displayed in Fig. 1.

Figs. 2 and 3 contain images of the bound Alexa Fluor 660-labelled anti-fluorescein $F(ab')_2$ layer within fluorescein functionalised Streamline agarose beads for two different incubation times. Fig. 2 shows overlayed images from the fluorescein and Alexa Fluor 660 detection channels and therefore show a dual-colour pattern. Images for both adsorbents (8.2 μmol immobilised fluorescein/mL beads and 0.92 μmol immobilised fluorescein/mL beads) are presented in Fig. 2. It can be seen that for the adsorbent with the higher immobilised ligand loading, these images are characterised by three distinct zones:

(i) A thin outer red layer that derives from the fluorescence emanating from the Alexa Fluor 660 moiety of the dye-conjugated anti-fluorescein $F(ab')_2$.
(ii) Deeper inside the scanned cross-section of the bead colour overlap occurs between the dual fluorescence emissions from the Alexa Fluor 660-labelled anti-fluorescein $F(ab')_2$ and unbound immobilised fluorescein. The resulting

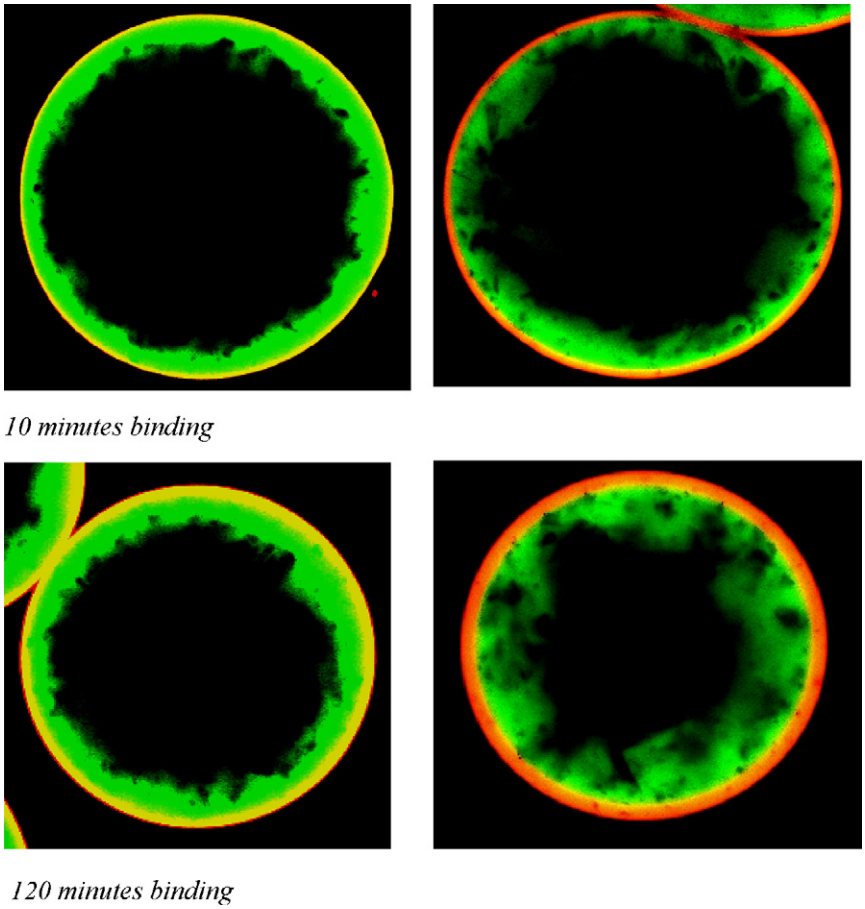

Fig. 2. Confocal scans of Streamline agarose beads with 8.2 μmol/mL beads of immobilised fluorescein ligand (left) and 0.92 μmol/mL beads of immobilised fluorescein ligand (right). The images are overlays of fluorescence scans in two separate detection channels corresponding to fluorescein and Alexa Fluor dyes. The images show three colour regions: (i) an outer ring of red colour representing immobilised ligand sites saturated with bound $F(ab')_2$, (ii) an intermediate region of yellow colour, representing immobilised ligand sites which are not yet completely saturated but still contain bound anti-fluorescein $F(ab')_2$ and (iii) an inner region of green colour, which represents fresh, unused immobilised ligand sites. It can be observed that the intermediate yellow region (ii) is practically undetectable in the adsorbent with lower immobilised ligand loading (right).

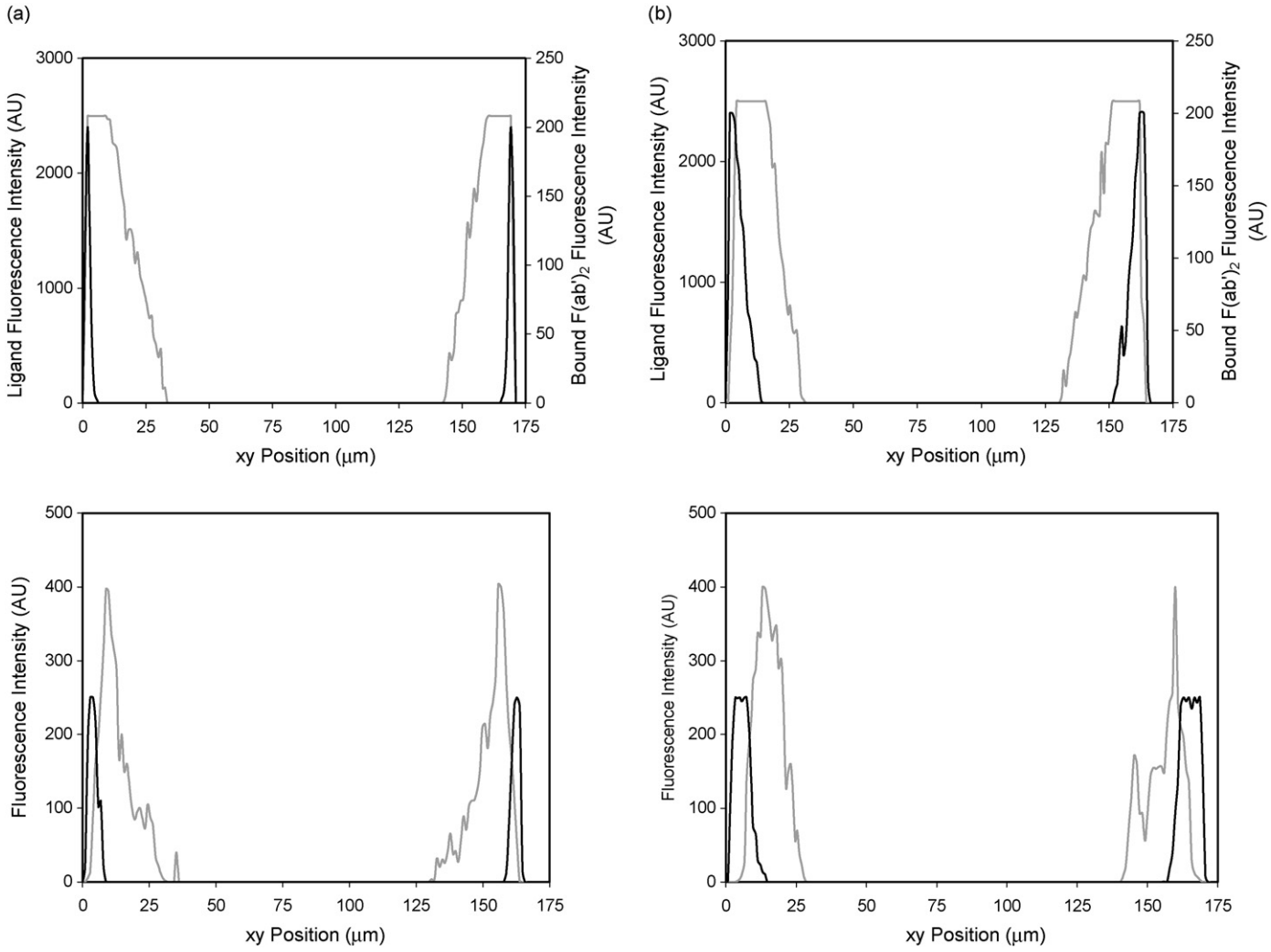

Fig. 3. Dual fluorescence intensity profiles obtained for Alexa Fluor 660-labelled anti-fluorescein F(ab′)$_2$ bound onto Streamline agarose beads activated with immobilised fluorescein at incubation times of (a) 10 min and (b) 120 min. Top profiles correspond to adsorbent beads with immobilised ligand loading of 8.2 μmol fluorescein/mL beads and bottom profiles correspond to adsorbent beads with 0.92 μmol fluorescein/mL beads. The images show how the relative immobilised ligand utilisation is higher in the adsorbent with low immobilised ligand loading than the adsorbent with higher immobilised ligand loading for the same incubation times (10 and 120 min incubation). This is indicated by the higher quenching of fluorescein binding sites on the outer edges of the beads observed in the profiles corresponding to the beads with immobilised ligand loading of 0.92 μmol fluorescein/mL of beads ((a) bottom and (b) bottom). Only the fluorescence data obtained from the Alexa Fluor 660 emission channel was used for quantitative analysis of the progressive depth of bound anti-fluorescein F(ab′)$_2$. Ligand fluorescence was used on a qualitative, comparative basis as a means of observing relative ligand utilisation in the two groups of adsorbents.

yellow region becomes progressively broader as adsorption proceeds.

(iii) At yet deeper penetration the green fluorescein fluorescence indicates the unbound binding sites of the immobilised fluorescein layer where no dye-labelled F(ab′)$_2$ has yet penetrated.

The images of the adsorbent with a 9-fold lower immobilised ligand loading (0.92 μmoles immobilised fluorescein/mL beads) are different. Fluorescence quenching is a characteristic property of the fluorescein/anti-fluorescein system and provides a sensitive measure of antibody-antigen binding in a solution phase immuno-chemical assay [15]. In the images in Fig. 2 (right) the lack of fluorescein fluorescence arises from the saturation of the outer ligand sites by Alexa Fluor 660-labelled anti-fluorescein F(ab′)$_2$. The intermediate yellow region (ii) corresponding to incomplete saturation of the fluorescein ligand sites is practically undetectable. Only the complete saturation region (i) and the free, unused ligand region (iii) are distinguishable with progressive thickening of the region of saturated Alexa Fluor 660-labelled anti-fluorescein F(ab′)$_2$ adsorption. The absence of a region of colour overlap (region (ii)) in these images indicates that binding of F(ab′)$_2$ to the immuno-affinity adsorbent with lower immobilised antigen density results in a more efficient immobilised ligand utilisation [10].

The relative immobilised ligand utilisation in adsorbent beads with immobilised fluorescein loadings of 8.2 μmol fluorescein/mL and 0.92 μmol fluorescein/mL were monitored by means of the respective fluorescence intensity profiles obtained for the bound Alexa Fluor 660-labelled anti-fluorescein F(ab′)$_2$ layer in each case. The fluorescence

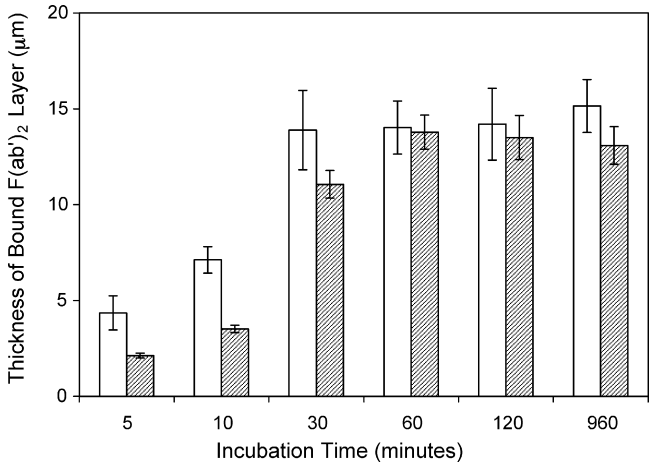

Fig. 4. The variation of bound $F(ab')_2$ layer thickness based on the intensity profiles of Alexa Fluor 660-labelled anti-fluorescein $F(ab')_2$ layer following different binding times for (□) adsorbent with 0.92 μmol fluorescein/mL beads and (▨) adsorbent with 8.2 μmol fluorescein/mL beads.

intensity profiles corresponding for the shortest incubation time of 10 min and the longest incubation time of 2 h are shown in Fig. 3. The dual fluorescence intensity profiles indicate that the immobilised ligand utilisation is more efficient in the case of the adsorbent with lower ligand loading (0.92 μmol immobilised fluorescein/mL adsorbent). It is clear from the fluorescence intensity profiles corresponding to this adsorbent that a more complete saturation of immobilised fluorescein sites occurs as indicated by the fluorescence quenching detected in the fluorescein emission channel. The fluorescence profiles resulting from the Alexa Fluor 660 emission channel were used to monitor the progressive depth of the bound anti-fluorescein $F(ab')_2$ layer in each adsorbent with respect to time and the results are shown in Fig. 4. It could be observed from Fig. 4 that $F(ab')_2$ penetration within the adsorbent with 0.92 μmol immobilised fluorescein/mL is initially more rapid than that within the adsorbent with a 9-fold higher load of immobilised fluorescein (8.2 μmol fluorescein/mL beads). These results could be attributed to steric hindrance effects; in the particular case of the binding of proteins onto considerably smaller immobilised molecules (such as haptens), steric hindrance effects acquire conspicuous proportions [10]. In the present study, the difference in molecular weight between the ligand and the protein is significant (×250); therefore steric hindrance effects are likely to have become more discriminatory and would tend to render the exploitation of high ligand density to any profitable extent impossible. To illustrate this, it is possible to estimate the average distance between two neighbouring ligands, S, by the following formula [17]:

$$S = \left(\frac{A}{L_t N_A}\right)^{1/2} \quad (1)$$

A is the surface area of the adsorbent (g/m^2), L_t the total immobilised ligand concentration (mM) and N_A is Avogadro's number. In our example, taking the surface area for Streamline™ agarose as 42 m^2/g (as estimated by the manufacturer based on an approximation to the surface area of Sepharose), the average distance between 2 adjacent ligand sites according to this equation would be 2.9 nm for the adsorbent with 8.2 μmol immobilised fluorescein/mL beads and 8.7 nm for the adsorbent with 0.92 μmol immobilised fluorescein/mL beads. This distance is much smaller than the maximum distance between the 2 Fab arms (20 nm), observed when the antibody reacts with the antigen [18]. If we assume the $F(ab')_2$ molecule to be a sphere with 20 nm radius, whenever a $F(ab')_2$ molecule binds to a ligand site on the adsorbent with 8.2 μmol/mL beads, up to 6 adjacent binding sites become masked by the bound molecule. Compared to that, only 2 adjacent binding sites would be masked by the bound molecule when the adsorbent with 0.92 μmol immobilised fluorescein/mL beads is used.

Adsorption of Alexa Fluor 660 conjugated anti-fluorescein $F(ab')_2$ to immobilised fluorescein was also imaged in the presence of serum digests. The fluorescence profiles for both

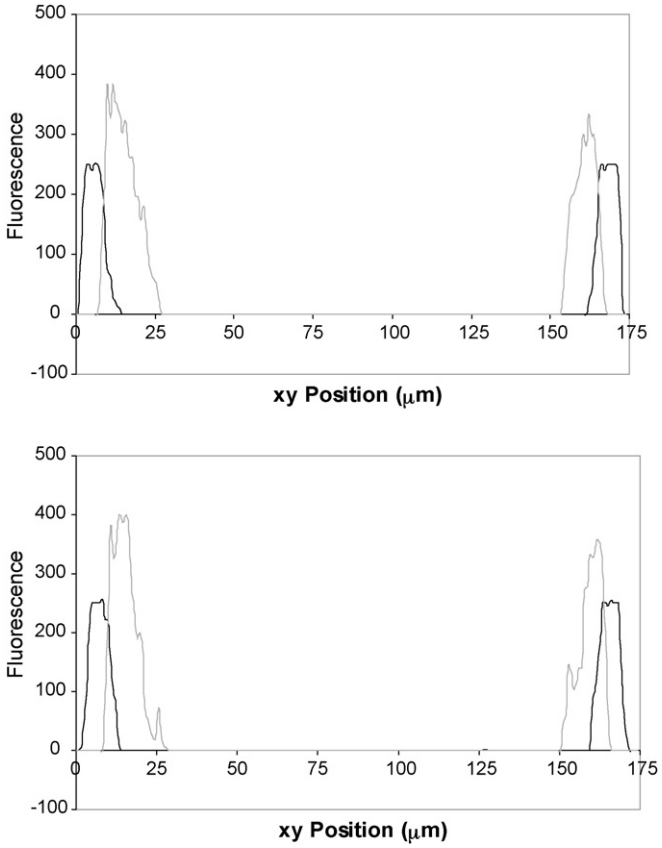

Fig. 5. Fluorescence intensity profiles for immobilised fluorescein ligand (dashed line) and the binding of anti-fluorescein $F(ab')_2$, labelled with red fluorescent dye Alexa Fluor 660 (solid line) in: (a) the presence and (b) absence of serum digests after 60 min incubation with Streamline agarose beads with 0.92 μmol fluorescein/mL beads density of immobilised fluorescein ligand. It is clear from the profiles that no significant difference in the penetration profile results from processing the complex mixture of serum digests. It can also be seen from the profiles that significant fluorescence quenching occurs at the outside of the bead (indicated by the shift of the immobilised ligand fluorescence profile towards the centre). This is in agreement with the confocal images which show a better immobilised ligand utilisation in the case of the adsorbent with lower ligand loading (Fig. 2).

cases are illustrated in Fig. 5. The Alexa Fluor 660-labelled anti-fluorescein $F(ab')_2$ samples were mixed with anti-fluorescein-free serum digest solutions to synthesise more industrially-relevant samples and also to investigate the effects of the presence of such a complex mixture of proteins on the binding of anti-fluorescein $F(ab')_2$. The red fluorescence detected in the resulting images was only due to anti-fluorescein $F(ab')_2$ because the conjugation of the fluorescent dye was carried out on the immuno-affinity purified anti-fluorescein $F(ab')_2$ sample prior to mixing it with the anti-fluorescein-free serum digest. The fluorescence profiles in Fig. 5 correspond to 60 min binding time and show no differences in the adsorption of $F(ab')_2$ samples prepared in serum digest and $F(ab')_2$ samples prepared in blank buffer. It can also be seen from the profiles that more efficient utilisation of immobilised ligand is achieved as demonstrated by the fluorescence quenching observed in the fluorescein intensity profile at the outer edges of the beads. This significant fluorescence quenching indicates a greater saturation of the immobilised fluorescein sites by the bound anti-fluorescein $F(ab')_2$. The effective diffusivity coefficients for $F(ab')_2$ transport within the adsorbent particles in the presence and absence of serum digest fragments were estimated by applying the shrinking core mechanism assumptions [16]. Yoshida et al. were able to fit their rate data for the adsorption of a protein onto Chitosan beads to the conventional shrinking core model [19]. Here, it can be assumed that pore diffusion is the controlling step in the adsorption, as has been shown for protein adsorption within similar adsorbents [20]. The binding of anti-fluorescein to immobilised fluorescein at the surface of the adsorbent bead can further be assumed to be faster than diffusion inside the outer layer due to the high Ab–Ag binding affinity. In addition, the concentration of anti-fluorescein $F(ab')_2$ in the bulk solution remains approximately constant throughout the adsorption process because it is in excess compared to the total number of ligand binding sites available (×5 excess). The confocal profiles were hence used to calculate the thickness of the shrinking core at various adsorption time points and use those values to calculate the effective diffusivity coefficient for the transport of anti-fluorescein $F(ab')_2$ within the immuno-affinity adsorbent beads with 0.92 μmol immobilised fluorescein/mL by applying the shrinking core equation for pore diffusion control [21] (Fig. 6):

$$t = \frac{C_{Ag_0} R^2}{6 b D_e C_{Ab_0}} \left[1 - 3\left(\frac{r_c}{R}\right)^2 + 2\left(\frac{r_c}{R}\right)^3 \right] \quad (2)$$

where t is the time (s), b the stoichiometric factor (1:2), C_{Ab_0} the concentration of anti-FITC $F(ab')_2$ in solution (M), C_{Ag_0} the ligand density on the adsorbent particle (M), D_e the diffusion coefficient (m^2/s), r_c radius of the unreacted shrinking core (m) and R particle radius occupied by immobilised ligand (m). The results are shown in Fig. 5. The value of the effective diffusivity coefficient inside the adsorbent was estimated to be $1.5 \pm 0.06 \times 10^{-12}\ m^2\ s^{-1}$ for $F(ab')_2$ adsorption from crude serum digest and $1.2 \pm 0.05 \times 10^{-12}\ m^2\ s^{-1}$ for pre-purified $F(ab')_2$ adsorption. The error bars shown on Fig. 5 represent the variation in the data obtained from images of 3 different sample beads. These values indicate that the presence of serum digest fragments has little or no effect upon the diffusivity of $F(ab')_2$ inside the immuno-affinity adsorbent to any significant extent. Diffusion coefficients calculated from the pore diffusion model for transport of IgG through different types of chromatographic media have been reported in the literature [22–25]. The values reported show a wide range of variety, which reflects the importance of the adsorbent used, the antibody system and purification conditions in the estimation of diffusivity coefficients. Some of the diffusivity coefficients reported for the same initial IgG liquid phase concentration as the concentration used in our experiments were 100-fold higher than the value estimated from our experiments for porous glass based supports and 30-fold higher than the values estimated from agarose [25] and Silica-Dextran [23] based supports. Furthermore, it was expected that the diffusivity coefficient of $F(ab')_2$ would be higher than that of the heavier IgG, however our results showed a lower diffusion coefficient for the fluorescent dye-conjugated $F(ab')_2$ than that of intact IgG. The significant difference between our results and the published values might be explained by the structural difference between $F(ab')_2$ and IgG. It has been suggested in some studies that the Fc region, which is absent in $F(ab')_2$ fragments, may influence the antibody binding characteristics in solid-phase system, possibly by influencing antibody flexibility and hence impairing the $F(ab')_2$ ability to penetrate through the bound $F(ab')_2$ layer [26]. It is also possible that the conjugation of the fluorescent probe added to these structural changes. However, it is unlikely that this has resulted in a decrease in the binding affinity of the conjugated $F(ab')_2$ molecules compared with their un-conjugated counterparts, because if there was an overshoot of un-conjugated $F(ab')_2$ towards the centre of the beads, the confocal images would have shown an antigen binding-induced fluorescence quenching in that region. Clearly, the fluorescence profiles do not provide conclusive information about the mass transfer kinetics of the system, a more accurate estimate of the diffusivity coefficients can be obtained by using the fluorescence profiles in conjunction with uptake measurements for the

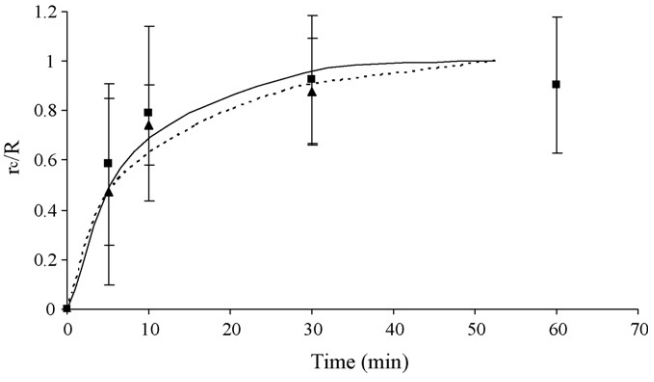

Fig. 6. Fit of the shrinking core model for pore diffusion control to confocal fluorescence profile data obtained for serum digest adsorption [(■) data, (—) model] and pre-purified $F(ab')_2$ adsorption [(▲) data, (- - -) model].

system under consideration. Previous studies have determined the spatially integrated fluorescence intensity to quantify protein adsorption in homogeneous gel phase adsorbents [10].

4. Conclusion

This study aimed to utilise dual fluorescence confocal scanning laser microscopy in order to visualise the accessibility and binding patterns of Alexa Fluor 660-conjugated anti-fluorescein $F(ab')_2$ to fluorescein immobilised on Streamline agarose; an adsorbent ubiquitously used in expanded bed chromatography and other purification modes where good fluidisation properties and rapid settling velocities are essential. Two batches of this immuno-affinity adsorbent were synthesised, each one containing a different loading of immobilised fluorescein ligand. The resulting dual fluorescence intensity profiles revealed that the higher immobilised ligand density (8.2 μmol/mL beads) resulted in a marked decrease in the utilisation of immobilised ligand. The diffusion of the anti-fluorescein $F(ab')_2$ front through the adsorbent beads appeared to obey the shrinking core model in the case of the adsorbent with the lower ligand loading (0.92 μmol immobilised fluorescein/mL beads) but not for high ligand loading adsorbent with 8.2 μmol/mL beads ligand density. In the latter case, an intermediate region of incomplete saturation was observed that is unaccounted for by the shrinking core model. Estimates of effective diffusion coefficients based on the shrinking core mechanism were obtained for adsorption of anti-fluorescein $F(ab')_2$ in the presence and absence of serum digest fragments. The effective diffusivity values were similar for both cases indicating that the serum digest fragments have no marked effect upon the diffusion of $F(ab')_2$ inside the immuno-adsorbent under these experimental conditions.

Confocal microscopy was found to be a convenient technique to gain insight in intra-particle protein adsorption within Streamline agarose containing various immobilised ligand loadings, however the technique could only be used on a comparative, semi-quantitative basis due to the non-homogeneity of the resin. The non-homogeneity of Streamline matrices is inherent to their stable fluidisation and mechanical rigidity properties, which result from the quartz particles embedded within the matrix. However, the quantitative potential of the dual fluorescence technique described here could be enhanced by using a more uniform and homogeneous matrix such as Sepharose in order to obtain absolute values for the effect of immobilised ligand concentration on protein uptake.

Acknowledgements

The main author thanks The Algerian Ministry of Higher Education for providing a scholarship during the tenure of which this work has been conducted. Special thanks to Mr. Rowan Hooper and Mr. Alex Domin for assistance in operating the confocal microscope. We are equally grateful to Micro-Pharm Ltd. (Emlyn, UK) for the supply of the anti-fluorescein sheep serum and to the EPSRC for funding the project.

References

[1] Theakston RDG, Smith DC. Therapeutic antibodies. London: Springer; 1995. p. 109.
[2] Rojas G, Jimenez JM, Gutierrez JM. Caprylic-acid fractionation of hyperimmune horse plasma: description of a simple procedure for antivenom production. Toxicon 1994;32:351–63.
[3] Knuden HL, Fahrner RL, Xu Y, Norling LA, Blank GS. Membrane ion-exchange chromatography for process-scale antibody purification. J Chromatogr A 2001;907:145–54.
[4] Boschetti E. The use of thiophilic chromatography for antibody purification: a review. J Biochem Biophys Methods 2001;49:361–89.
[5] Lowe CR, Lowe AR, Gupta G. New developments in affinity chromatography with potential application in the production of biopharmaceuticals. J Biochem Biophys Methods 2001;49(1–3):561–74.
[7] Theakston RDG, Smith DC. Antivenoms—a review of current status and future developments. Biodrugs 1997;7:366–75.
[8] Krifi MN, El Ayeb M, Dellagi K. The improvement and standardization of antivenom production in developing countries: comparing antivenom quality, therapeutical efficiency, and cost. J Venom Anim Toxins 1999;5(2):128–41.
[9] Chase HA. The use of affinity adsorbents in expanded bed adsorption. J Mol Recog 1998;11(1–6):217–21.
[10] Ljunglöf A, Larsson M, Knuuttila KG, Lindgren J. Measurement of ligand distribution in individual adsorbent particles using confocal scanning laser microscopy and confocal micro-Raman spectroscopy. J Chromatogr A 2000;893(2):235–44.
[11] Kumpalume P, Boushaba R, Jones RGA, Slater NKH. Facile $F(ab')_2$ manufacturing: strategies for the production of snake antivenoms. Trans (IChemE) 2002;80[C]:88–97.
[12] Sundberg L, Porath I. Preparation of addsorbents for biospecific affinity chromatography. J Chromatogr A 1974;90:87–98.
[13] Boushaba R, Kumpalume P, Slater NKH. Kinetics of whole serum and pre-purified IgG digestion by pepsin for $F(ab')_2$ manufacture. Biotechnol Prog 2003;19(4):1176–82.
[14] Li P, Xiu G, Rodrigues AE. Modeling breakthrough and elution curves in fixed bed of inert core adsorbents: analytical and approximate solutions. Chem Eng Sci 2004;59(15):3091–103.
[15] Lopatin DE, Voss Jr EW. Fluorescein: hapten and antibody active site probe. Biochemistry 1971;10(2):208–13.
[16] Pritzker MD. Model for parallel surface and pore diffusion of an adsorbate in a spherical adsorbent particle. Chem Eng Sci 2003;58(2):473–8.
[17] Wu DL, Walters RR. Effects of stationary phase ligand density on high performance ion exchange chromatography. J Chromatogr A 1992;598:7–13.
[18] Freinstein A, Rowe AJ. Molecular mechanism of formation of antigen-antibody complex. Nature 1965;205:147–9.
[19] Yoshida H, Yoshikava M, Kataokal T. Parallel transport of BSA by surface and pore diffusion in strongly basic Chitosan. AIChE J 1994;40(12):2034–44.
[20] Weaver Jr LE, Carta G. Protein adsorption on cation exchangers: Comparison of macroporous and gel-composite media. Biotechnol Prog 1996;12(3):342–55.
[21] Levenspiel O. Chemical reaction engineering. New York: John Wiley & Sons Inc; 1972. p. 364.
[22] McCue JT, Kemp G, Low D, Quiñones-García I. Evaluation of protein A chromatography media. J Chromatogr A 2003;989(1):139–53.
[23] Chen WD, Dong XY, Sun YJ. Analysis of diffusion models for protein adsorption to porous anion exchange adsorbent. J Chromatogr A 2002;962:29–40.
[24] Pai A, Gondkar S, Lali A. Enhanced performance of expanded bed chromatography on rigid superporous adsorbent matrix. J Chromatogr A 2000;867:113–30.
[25] Tscheliessnig A, Hahn R, Jungbauer A. In situ determination of adsorption kinetics of proteins in a finite bath. J Chromatogr A 2005;1069(1):23–30.
[26] McCloskey N, Turner MW, Goldblatt D. Correlation between the avidity of mouse-human chimeric IgG subclass monoclonal antibodies measured by solid-phase elution ELISA and biospecific interaction analysis (BIA). J Immunol Methods 1997;205(1):67–72.